Invariant Extended Kalman Filtering Using Two Position Receivers for Extended Pose Estimation

Natalia Pavlasek[1], Alex Walsh[2], and James Richard Forbes[3]

Abstract— This paper considers the use of two position receivers and an inertial measurement unit (IMU) to estimate the position, velocity, and attitude of a rigid body, collectively called extended pose. The measurement model consisting of the position of one receiver and the relative position between the two receivers is left invariant, enabling the use of the invariant extended Kalman filter (IEKF) framework. The IEKF possesses various advantages over the standard multiplicative extended Kalman filter, such as state-estimate-independent Jacobians. Monte Carlo simulations demonstrate that the two-receiver IEKF approach yields improved estimates over a two-receiver multiplicative extended Kalman filter (MEKF) and a single-receiver IEKF approach. An experiment further validates the proposed approach, confirming that the two-receiver IEKF has improved performance over the other filters considered.

I. INTRODUCTION

Estimating robot position, velocity, and attitude, collectively referred to as extended pose [1], is typically accomplished by fusing interoceptive and exteroceptive sensor data together using a nonlinear filter. Common interoceptive sensors are accelerometers and rate gyros. GPS receivers, or more generally GNSS receivers, ultra-wideband (UWB) receivers, and long baseline (LBL) acoustic arrays are common exteroceptive positioning sensors used for outdoor, indoor, and underwater navigation, respectively. The problem of estimating extended pose using an accelerometer, a rate gyro, and two position receivers, referred to as the two-receiver extended pose estimation problem, is the focus of this paper. This sensor suite is widely available, has improved observably properties relative to a one-receiver set-up, and depending on the application domain, the navigation solution proposed herein can be applied in outdoor, indoor, and underwater scenarios.

The two-receiver extended pose estimation problem has many solutions that can be split into tightly-coupled and loosely-coupled approaches. Tightly coupled approaches such as the carrier-phase approach [2–5] or pseudorange approach [6] are effective, but add complexity. For example, resolution of the integer ambiguity problem is required [4]. Loosely-coupled receiver-INS solutions are simpler to implement, and are effective for rapid deployment of estimation algorithms. While solutions using extended Kalman filters

(EKFs) exist for the loosely-coupled problem [7, 8], new developments in state estimation, such as the invariant EKF (IEKF) [9], warrant a second look at the two-receiver problem.

The particle filter (PF), the unscented Kalman filter (UKF), the EKF, and many other filters, are approximations of the Bayes filter [10]. The IEKF is a variant of the EKF that takes advantage of the symmetry of matrix Lie groups that naturally arises in attitude, pose (i.e., position and attitude), and extended pose estimation problems. Several desirable properties arise from the symmetry-preserving nature of the system. For instance, provided certain conditions are met, the IEKF state-estimation error is independent of the true vehicle trajectory [11]. Moreover, the IEKF is guaranteed to converge locally under certain assumptions [11]. The IEKF has improved transient response over the MEKF, especially with large initial errors [9, 11, 12]. As such, the goal of this paper is to leverage the IEKF in the two-receiver extended pose estimation problem. The novel contribution of this paper is demonstrating how to use an accelerometer, a rate gyro, and two position receivers to estimate position, velocity, and attitude within the IEKF framework. The proposed two-receiver IEKF is compared to a two-receiver MEKF, similar to [6, 8], in both simulation and experiment. The experiments presented use position measurements from a UWB system. UWB is a highly accurate positioning system that can be used in GPS denied environments [13], and that does not suffer from long-term drift [14].

The remainder of this paper is organized as follows. Section II reviews some preliminaries, namely matrix Lie group theory, the IEKF equations, and the average normalized innovation squared (NIS) test. Section III introduces the problem and summarizes the equations of motion before framing the problem in the IEKF framework. Section IV presents the findings from simulations and an experiment. Finally, Section V provides concluding remarks.

II. PRELIMINARIES

A. Matrix Lie Groups

Consider the matrix Lie group $\mathcal{G}$ composed of $n \times n$ invertible matrices with m degrees of freedom that is closed under matrix multiplication [15]. The matrix Lie algebra associated with $\mathcal{G}$ is denoted $\mathfrak{g}$. An element of $\mathfrak{g}$ can be mapped to $\mathcal{G}$ using the exponential map, $\exp(\cdot) : \mathfrak{g} \to \mathcal{G}$. Similarly, an element of $\mathcal{G}$ can be mapped to $\mathfrak{g}$ using the matrix natural logarithm, $\log(\cdot) : \mathcal{G} \to \mathfrak{g}$. The linear operator $(\cdot)^\wedge$ maps $\mathbb{R}^m \to \mathfrak{g}$, and $(\cdot)^\vee$ maps $\mathfrak{g} \to \mathbb{R}^m$. When

$\delta\boldsymbol{\xi} \in \mathbb{R}^m$ is small, $\exp\left(\delta\boldsymbol{\xi}^\wedge\right)$ can be approximated as $\exp\left(\delta\boldsymbol{\xi}^\wedge\right) \approx \mathbf{1} + \delta\boldsymbol{\xi}^\wedge$.

B. Invariant Extended Kalman Filtering Preliminaries

The IEKF framework has four conditions that must be met for it to be used. First, the measurement model must be either left or right invariant. The second and third conditions are that the invariant error and invariant innovation must be consistent with the left or right invariance of the measurement model. Fourth, the process model must be group affine. In this section, each of these components will be discussed, with a focus on left invariance.

Definition 2.1 (Left-Invariant Measurement Model [9]): Consider a measurement $\mathbf{y}_k \in \mathbb{R}^n$, a state $\mathbf{X}_k \in \mathcal{G} \subset \mathbb{R}^{n\times n}$, where $\mathcal{G}$ is a matrix Lie group, a known column matrix $\mathbf{b} \in \mathbb{R}^n$, and zero-mean Gaussian white noise $\mathbf{n}_k \in \mathbb{R}^n$. A left-invariant measurement model is defined by

$$\mathbf{y}_k = \mathbf{X}_k \mathbf{b} + \mathbf{n}_k. \tag{1}$$

Definition 2.2 (Left-Invariant Error [9]): Let $\mathbf{X}_k \in \mathcal{G}$ be the true state of a system, $\bar{\mathbf{X}}_k \in \mathcal{G}$ be a state different from the true state, such as the predicted or corrected state estimates. The left invariant error is defined by

$$\delta\mathbf{X}_k = \mathbf{X}_k^{-1}\bar{\mathbf{X}}_k. \tag{2}$$

Definition 2.3 (Left-Invariant Innovation [9]): Let $y_k \in \mathbb{R}^n$ be the predicted measurement, and $\mathbf{z}_k \in \mathbb{R}^n$ be the innovation. The left-invariant innovation is given by

$$\mathbf{z}_k = \check{\mathbf{X}}_k^{-1}(\mathbf{y}_k - \check{\mathbf{y}}_k). \tag{3}$$

Definition 2.4 (Group Affine [9]): A function $\mathbf{F}(\mathbf{X}, \mathbf{u})$ is said to be group affine if for all $\mathbf{X}_1, \mathbf{X}_2 \in \mathcal{G}$ and $\mathbf{u} \in \mathbb{R}^{n_u}$, the equation

$$\mathbf{F}(\mathbf{X}_1\mathbf{X}_2, \mathbf{u}) = \mathbf{X}_1\mathbf{F}(\mathbf{X}_2, \mathbf{u}) + \mathbf{F}(\mathbf{X}_1, \mathbf{u})\mathbf{X}_2 - \mathbf{X}_1\mathbf{F}(\mathbf{1}, \mathbf{u})\mathbf{X}_2 \tag{4}$$

is satisfied.

Given the left-invariant measurement model Definition 2.1, error given by Definition 2.2, innovation from Definition 2.3, and a process model that satisfies Definition 2.4, the IEKF framework can be used [9].

C. Invariant Extended Kalman Filtering Implementation

Consider a process model of the form

$$\dot{\mathbf{X}}(t) = \mathbf{F}(\mathbf{X}(t), \mathbf{u}(t)) + \mathbf{X}(t)\mathbf{W}(t), \tag{5}$$

where $\mathbf{F}(\mathbf{X}(t), \mathbf{u}(t))$ is group affine, $\mathbf{X}(t) \in \mathcal{G}$, $\mathbf{u}(t) \in \mathbb{R}^{n_u}$ is the process input, and $\mathbf{W}(t) = \mathbf{w}(t)^\wedge \in \mathfrak{g}$ is zero-mean Gaussian white process noise. For the remainder of this work, the argument (t) is dropped for conciseness, unless required for clarity. The nonlinear process model can be linearized using the definition of the left-invariant error (2) to yield

$$\delta\dot{\boldsymbol{\xi}} = \mathbf{A}_c\delta\boldsymbol{\xi} + \mathbf{L}_c\delta\mathbf{w}, \tag{6}$$

where $\delta\mathbf{w} \sim \mathcal{N}(\mathbf{0}, \boldsymbol{Q}\delta(t - \tau))$, and $\boldsymbol{Q}$ is the power spectral density. The discrete time prediction is then

$$\check{\mathbf{X}}_k = \mathbf{F}_{k-1}(\hat{\mathbf{X}}_{k-1}, \mathbf{u}_{k-1}), \tag{7}$$

$$\check{\mathbf{P}}_k = \mathbf{A}_{k-1}\hat{\mathbf{P}}_{k-1}\mathbf{A}_{k-1}^\mathsf{T} + \mathbf{L}_{k-1}\mathbf{Q}_{k-1}\mathbf{L}_{k-1}^\mathsf{T}, \tag{8}$$

where (7) comes from discretization of (5), and $\mathbf{A}_{k-1}$, $\mathbf{L}_{k-1}$, and $\mathbf{Q}_{k-1}$ come from discretization of (6) and $\boldsymbol{Q}$ [16]. The left-invariant innovation can be linearized, again using the definition of the left-invariant error (2), along with the approximation $\delta\mathbf{X}_k = \exp(\delta\boldsymbol{\xi}_k^\wedge) \approx \mathbf{1} + \delta\boldsymbol{\xi}_k^\wedge$. In detail,

$$\mathbf{z}_k = \check{\mathbf{X}}_k^{-1}(\mathbf{X}_k\mathbf{b} + \mathbf{n}_k - \check{\mathbf{X}}_k\mathbf{b}) = \delta\mathbf{X}_k^{-1}\mathbf{b} - \mathbf{b} + \check{\mathbf{X}}_k^{-1}\mathbf{n}_k$$
$$\approx (\mathbf{1} - \delta\boldsymbol{\xi}_k^\wedge)\mathbf{b} - \mathbf{b} + \check{\mathbf{X}}_k^{-1}\delta\mathbf{n}_k = \mathbf{H}_k\delta\boldsymbol{\xi}_k + \mathbf{M}_k\delta\mathbf{n}_k. \tag{9}$$

where $\mathbf{M}_k = \check{\mathbf{X}}_k^{-1}$ and $\delta\mathbf{n}_k \sim \mathcal{N}(\mathbf{0}, \mathbf{R}_k)$. The state correction is then

$$\hat{\mathbf{X}}_k = \check{\mathbf{X}}_k \exp\left(-(\mathbf{K}_k\mathbf{z}_k)^\wedge\right), \tag{10}$$

which is consistent with the definition of the left-invariant error in (2). The Kalman gain is

$$\mathbf{K}_k = \check{\mathbf{P}}_k\mathbf{H}_k^\mathsf{T}\mathbf{S}_k^{-1}, \tag{11}$$

where

$$\mathbf{S}_k = \mathbf{H}_k\check{\mathbf{P}}_k\mathbf{H}_k^\mathsf{T} + \mathbf{M}_k\mathbf{R}_k\mathbf{M}_k^\mathsf{T}. \tag{12}$$

D. Normalized Innovation Squared Test

The normalized innovation squared (NIS) is defined as [17, 18]

$$\epsilon_{z,k} = \mathbf{z}_k^\mathsf{T}\mathbf{S}_k^{-1}\mathbf{z}_k, \tag{13}$$

where $\mathbf{S}_k$ is given in (12). The NIS is χ^2 distributed of degree n_z. The average NIS,

$$\bar{\epsilon}_{z,k} = \frac{1}{N}\sum_{i=1}^{N}\epsilon_{z,k}^i, \tag{14}$$

is also χ^2 distributed of degree Nn_z, and can therefore be compared to the critical χ^2 values to verify the consistency of the estimator [17]. Dividing the result of (14) by n_z results in a values close to one for consistent systems [19]. A value greater than one indicates an optimistic estimator, where the errors to covariance ratio is too large, or the estimates include significant bias [17]. A value less than one indicates that the estimator is pessimistic.

III. THE TWO RECEIVER PROBLEM

A. Notation

The following notation is used throughout this work. A physical vector $\overrightarrow{p}$ resolved in $\mathcal{F}_a$ is denoted $\mathbf{p}_a$, and resolved in $\mathcal{F}_b$ is denoted as $\mathbf{p}_b$. The relationship between $\mathbf{p}_a$ and $\mathbf{p}_b$ is $\mathbf{p}_a = \mathbf{C}_{ab}\mathbf{p}_b$, or $\mathbf{p}_b = \mathbf{C}_{ba}\mathbf{p}_a$, where $\mathbf{C}_{ab} = \mathbf{C}_{ba}^\mathsf{T} = \mathbf{C}_{ba}^{-1} \in SO(3)$ is the direction cosine matrix (DCM). The cross product of two physical vectors resolved in a frame, such as $\mathcal{F}_b$, is denoted $\mathbf{p}_b^\times\mathbf{q}_b = -\mathbf{q}_b^\times\mathbf{p}_b$.

B. Problem Formulation

Consider a rigid body, with body frame $\mathcal{F}_b$, an inertial frame $\mathcal{F}_a$, and a datum point w. An IMU with an accelerometer and a rate gyro is mounted at point z_0 on the rigid body. Two position receivers, which could be GPS or UWB receivers, are placed at points z_1 and z_2, respectively, on the rigid body. The physical vector describing z_0 relative to w

is $\underset{\rightarrow}{r}^{z_0 w}$, and the physical vector describing z_1 relative to z_2 is denoted $\underset{\rightarrow}{r}^{z_1 z_2}$. The velocity of point z_0 relative to point w relative to $\mathcal{F}_a$ is $\underset{\rightarrow}{v}^{z_0 w/a}$.

The two-receiver extended pose estimation problem to be solved is, given an accelerometer, a rate gyro, and two position receivers, estimate the position, velocity, and attitude as described by $\mathbf{r}_a^{z_0 w}$, $\mathbf{v}_a^{z_0 w/a}$, and $\mathbf{C}_{ab}$, respectively. This problem follows a loosely-coupled GPS-INS formulation [17].

C. Measurement Models

The rate gyro, $\mathbf{u}_b^1$, and accelerometer, $\mathbf{u}_b^2$, measurement models are

$$\mathbf{u}_b^1 = \boldsymbol{\omega}_b^{ba} - \mathbf{w}_b^1, \tag{15}$$

$$\mathbf{u}_b^2 = \mathbf{C}_{ab}^{\mathsf{T}}(\dot{\mathbf{v}}_a^{z_0 w/a} - \mathbf{g}_a) - \mathbf{w}_b^2, \tag{16}$$

where $\boldsymbol{\omega}_b^{ba}$ is the angular velocity of $\mathcal{F}_b$ relative to $\mathcal{F}_a$ resolved in $\mathcal{F}_b$, $\dot{\mathbf{v}}_a^{z_0 w/a}$ is the acceleration of point z_0 relative to point w with respect to $\mathcal{F}_a$ resolved in $\mathcal{F}_a$, $\mathbf{g}_a$ is the gravity vector resolved in $\mathcal{F}_a$, and both $\mathbf{w}_b^1 \sim \mathcal{N}(0, \boldsymbol{Q}^{\omega}(t)\delta(t - \tau))$ and $\mathbf{w}_b^2 \sim \mathcal{N}(0, \boldsymbol{Q}^{\mathrm{a}}(t)\delta(t - \tau))$ are zero-mean Gaussian white measurement noise. Using (15) and (16) the continuous-time kinematic equations defining the time evolution of the rigid body are

$$\dot{\mathbf{C}}_{ab} = \mathbf{C}_{ab}(\mathbf{u}_b^1 + \mathbf{w}_b^1)^{\times}, \tag{17}$$

$$\dot{\mathbf{v}}_a^{z_0 w/a} = \mathbf{C}_{ab}(\mathbf{u}_b^2 + \mathbf{w}_b^2) + \mathbf{g}_a, \tag{18}$$

$$\dot{\mathbf{r}}_a^{z_0 w} = \mathbf{v}_a^{z_0 w/a}. \tag{19}$$

Biases are not included in (15) and (16), nor (17), (18), (19), because it is assumed that the sensor data has been calibrated such that biases are negligible, which is the case in the experiments presented in Section IV-B. Biases can be included in the "imperfect" IEKF framework [20, 21].

Position measurements from two position receivers affixed to the rigid body are available. Each position measurement is of the form

$$\mathbf{y}_k^{\mathrm{pos},i} = \mathbf{r}_{a_k}^{z_i w} + \mathbf{n}_k^{\mathrm{pos},i}, \quad i = 1, 2, \tag{20}$$

where $\mathbf{n}_k^i \sim \mathcal{N}(\mathbf{0}, \mathbf{R}^{z_i w})$. Subtracting the two position measurements yields a relative position measurement,

$$\mathbf{y}_k^{\mathrm{rel}} = \mathbf{y}_k^{\mathrm{pos},2} - \mathbf{y}_k^{\mathrm{pos},1} = \mathbf{r}_{a_k}^{z_2 w} - \mathbf{r}_{a_k}^{z_1 w} + \mathbf{n}_k^{\mathrm{rel}}, \tag{21}$$

where $\mathbf{n}_k^{\mathrm{rel}} = \mathbf{n}_k^{\mathrm{pos},2} - \mathbf{n}_k^{\mathrm{pos},1}$. Notice that $\mathbf{y}_k^{\mathrm{rel}}$ in (21) can be written

$$\mathbf{y}_k^{\mathrm{rel}} = \mathbf{C}_{ab_k} \mathbf{r}_b^{z_2 z_1} + \mathbf{n}_k^{\mathrm{rel}}, \tag{22}$$

where $\mathbf{r}_b^{z_2 z_1}$ is the known distance, the baseline, between the two receivers in $\mathcal{F}_b$. Some sensor suites, such as a moving baseline real-time kinematic (RTK) GPS system, will provide both (20) and (22) directly [22].

D. IEKF Formulation

The kinematic equations (17), (18), (19) can collectively be written using the group of double direct isometries, $SE_2(3)$ [9, 20], to form the IEKF process model. In particular,

$$\dot{\mathbf{X}} = \mathbf{F}(\mathbf{X}, \mathbf{u}_b) + \mathbf{X}\mathbf{W}_b \tag{23}$$

where $\mathbf{u}_b = [\mathbf{u}_b^{1^{\mathsf{T}}} \quad \mathbf{u}_b^{2^{\mathsf{T}}} \quad \mathbf{0}]^{\mathsf{T}}$, $\mathbf{W}_b^{\vee} = \mathbf{w}_b = [\mathbf{w}_b^{1^{\mathsf{T}}} \quad \mathbf{w}_b^{2^{\mathsf{T}}} \quad \mathbf{0}]^{\mathsf{T}}$,

$$\mathbf{X} = \begin{bmatrix} \mathbf{C}_{ab} & \mathbf{v}_a^{z_0 w/a} & \mathbf{r}_a^{z_0 w} \\ \mathbf{0} & 1 & 0 \\ \mathbf{0} & 0 & 1 \end{bmatrix} \in SE_2(3), \tag{24}$$

$$\mathbf{W}_b = \mathbf{w}_b^{\wedge} = \begin{bmatrix} \mathbf{w}_b^{1^{\times}} & \mathbf{w}_b^2 & \mathbf{0} \\ \mathbf{0} & 0 & 0 \\ \mathbf{0} & 0 & 0 \end{bmatrix} \in \mathfrak{se}_2(3), \tag{25}$$

$$\mathbf{F}(\mathbf{X}, \mathbf{u}_b) = \begin{bmatrix} \mathbf{C}_{ab}\mathbf{u}_b^{1^{\times}} & \mathbf{C}_{ab}\mathbf{u}_b^2 + \mathbf{g}_a & \mathbf{v}_a^{z_0 w/a} \\ \mathbf{0} & 1 & 0 \\ \mathbf{0} & 0 & 1 \end{bmatrix}. \tag{26}$$

The function (26) is group affine [9]. The subblocks composing the left-invariant error (2) between $\mathbf{X} \in SE_2(3)$ and $\hat{\mathbf{X}} \in SE_2(3)$ are

$$\delta\mathbf{C}_{ab} = \mathbf{C}_{ab}^{\mathsf{T}}\hat{\mathbf{C}}_{ab}, \tag{27}$$

$$\delta\mathbf{v}_a^{z_0 w/a} = \mathbf{C}_{ab}^{\mathsf{T}}(\hat{\mathbf{v}}_a^{z_0 w/a} - \mathbf{v}_a^{z_0 w/a}), \tag{28}$$

$$\delta\mathbf{r}_a^{z_0 w} = \mathbf{C}_{ab}^{\mathsf{T}}(\hat{\mathbf{r}}_a^{z_0 w} - \mathbf{r}_a^{z_0 w}). \tag{29}$$

These error definitions are used to linearize the process model, resulting in a linearized model of the form (6) where

$$\delta\boldsymbol{\xi} = \begin{bmatrix} \delta\boldsymbol{\xi}^{\theta^{\mathsf{T}}} & \delta\boldsymbol{\xi}^{v^{\mathsf{T}}} & \delta\boldsymbol{\xi}^{r^{\mathsf{T}}} \end{bmatrix}^{\mathsf{T}}, \tag{30}$$

and the Jacobians $\mathbf{A}_{\mathrm{c}}$ and $\mathbf{L}_{\mathrm{c}}$ are [20]

$$\mathbf{A}_{\mathrm{c}} = \begin{bmatrix} -\mathbf{u}_b^{1^{\times}} & \mathbf{0} & \mathbf{0} \\ -\mathbf{u}_b^{2^{\times}} & -\mathbf{u}_b^{1^{\times}} & \mathbf{0} \\ \mathbf{0} & \mathbf{1} & -\mathbf{u}_b^{1^{\times}} \end{bmatrix}, \tag{31}$$

$$\mathbf{L}_{\mathrm{c}} = \begin{bmatrix} -\mathbf{1} & \mathbf{0} & \mathbf{0} \\ \mathbf{0} & -\mathbf{1} & \mathbf{0} \\ \mathbf{0} & \mathbf{0} & \mathbf{0} \end{bmatrix}. \tag{32}$$

The Jacobian $\mathbf{A}_{\mathrm{c}}$ in (31) is independent of the state estimate. This is an attribute of group affine systems, a key ingredient in the IEKF framework. Additionally, $\mathbf{L}_{\mathrm{c}}$ in (32) happens to be constant and independent of the state estimate as well, although the IEKF framework does not guarantee this. The state-estimate independence of $\mathbf{A}_{\mathrm{c}}$ and $\mathbf{L}_{\mathrm{c}}$, that does not hold for the MEKF presented in Appendix-A, is an advantage of the IEKF that often results in better filter performance, in particular in the transient phase [9]. The continuous-time linearized process model is discretized using the method described in [16, 23].

The measurement model is composed of $\mathbf{y}_k^{\mathrm{pos},1}$, as defined in (20), and the relative position of two position receivers, as given in (21). Using (20) and (21), the measurement model is

$$\mathbf{y}_k = \begin{bmatrix} \mathbf{y}_k^1 \\ \mathbf{y}_k^2 \end{bmatrix}, \tag{33}$$

where

$$\mathbf{y}_k^1 = \begin{bmatrix} \mathbf{y}_k^{\text{pos},1} \\ 0 \\ 1 \end{bmatrix} = \mathbf{X}_k \begin{bmatrix} \mathbf{r}_b^{z_1 z_0} \\ 0 \\ 1 \end{bmatrix} + \begin{bmatrix} \mathbf{n}_k^{\text{pos},1} \\ 0 \\ 0 \end{bmatrix}, \quad (34)$$

$$\mathbf{y}_k^2 = \begin{bmatrix} \mathbf{y}_k^{\text{rel}} \\ 0 \\ 0 \end{bmatrix} = \mathbf{X}_k \begin{bmatrix} \mathbf{r}_b^{z_2 z_1} \\ 0 \\ 0 \end{bmatrix} + \begin{bmatrix} \mathbf{n}_k^{\text{rel}} \\ 0 \\ 0 \end{bmatrix}. \quad (35)$$

Both (34) and (35) composing (33) are left-invariant measurement models of form given in (1). The left-invariant innovation is then

$$\mathbf{z}_k = \begin{bmatrix} \mathbf{z}_k^1 \\ \mathbf{z}_k^2 \end{bmatrix} = \begin{bmatrix} \check{\mathbf{X}}_k^{-1} & \mathbf{0} \\ \mathbf{0} & \check{\mathbf{X}}_k^{-1} \end{bmatrix} \begin{bmatrix} \mathbf{y}_k^1 - \hat{\mathbf{y}}_k^1 \\ \mathbf{y}_k^2 - \hat{\mathbf{y}}_k^2 \end{bmatrix}. \quad (36)$$

The linearization of both $\mathbf{z}_k^i$, $i = 1, 2$ in (36) is accomplished using the definition of the left-invariant error (2) and the approximation $\delta \mathbf{X}_k = \exp(\delta \boldsymbol{\xi}_k^\wedge) \approx \mathbf{1} + \delta \boldsymbol{\xi}_k^\wedge$, as detailed in (9). The Jacobians in (9) specific to (36) are

$$\mathbf{H}_k = \begin{bmatrix} (\mathbf{r}_b^{z_1 z_0})^\times & \mathbf{0} & -\mathbf{1} \\ (\mathbf{r}_b^{z_2 z_1})^\times & \mathbf{0} & \mathbf{0} \end{bmatrix}, \quad \mathbf{M}_k = \begin{bmatrix} \check{\mathbf{C}}_{ab_k}^{-1} & \mathbf{0} \\ \mathbf{0} & \check{\mathbf{C}}_{ab_k}^{-1} \end{bmatrix}, \quad (37)$$

where redundant rows of zeros have been removed on both the left and right-hand sides of (9). The Jacobian $\mathbf{H}_k$ is independent of the state-estimate, as is guaranteed by the IEKF formulation, while Jacobian $\mathbf{M}_k$ is not state-estimate independent.

IV. SIMULATIONS AND EXPERIMENTS

The two-receiver IEKF is compared to a two-receiver multiplicative extended Kalman filter (MEKF), the performance of which is used as a baseline. Both the IEKF and MEKF use 9 states to represent the system. The single-receiver IEKF performance is also shown since the magnitude of the single-receiver errors help give context to the performance of the solutions of the two-receiver problem. The trajectories of the simulations and experiments are dynamic and excite sensors in all directions.

A. Simulations

100 Monte Carlo trials were run on the same 50 second trajectory. Each Monte Carlo trial introduces sensor noise, randomly sampled with the covariances from $\mathbf{Q}_{\text{d}} = \text{diag}\left(\mathbf{Q}_{\text{d}}^\theta, \mathbf{Q}_{\text{d}}^a\right)$, with $\mathbf{Q}_{\text{d}}^\theta = 0.0012^2 \times \mathbf{1}$ $(\text{rad})^2$ and $\mathbf{Q}_{\text{d}}^a = 0.0025^2 \times \mathbf{1}$ $(\text{m/s}^2)^2$. The initial positions and velocities are randomly sampled from $\hat{\mathbf{P}}_0 = \text{blkdiag}\left((\pi/3)^2 \times \mathbf{1}\ (\text{rad})^2, 0.1^2 \times \mathbf{1}\ (\text{m/s})^2, 0.1^2 \times \mathbf{1}\ (\text{m})^2\right)$. In order to highlight the advantage of the IEKF in the transient phase, a constant initial error of $\pi/3$ (rad) is introduced into each of the components of the attitude. The prediction step is performed at a frequency of 250 Hz, while the correction step is executed at 15 Hz. The RMSE in attitude, position and velocity for each Monte Carlo run was computed and reported in Fig. 1. The bars represent the average RMSE, while the upper and lower error bounds represent the 2.5
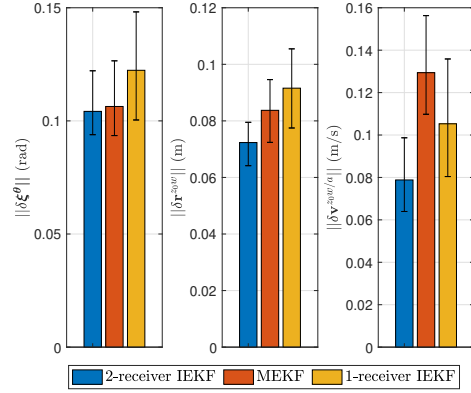

Fig. 1. Attitude, position, and velocity RMSE for two-receiver IEKF and MEKF, as well as one-receiver IEKF, for 100 simulated Monte Carlo runs.

and 97.5 percentile, respectively, meaning that 95% of trials lie between these bounds.

Fig. 1 shows that the two-receiver IEKF outperforms the two-receiver MEKF and single-receiver IEKF in its estimates of all states. These results are consistent with the literature, since the advantage of state-independent Jacobians emanates when the state estimates are highly erroneous, as is the case when the initial error is large. Thus, the steady state performance of the two-receiver IEKF and two-receiver MEKF should be similar, while the transient performance of the two-receiver IEKF should show improvement over the two-receiver MEKF [11]. Fig. 1 shows that the improvement in attitude is small, while the greater advantage arises in position and velocity estimates. The advantage arising from the two-receiver IEKF framework appears in the comparison of RMSE in velocity, where the single-receiver IEKF has lower RMSE than the two-receiver MEKF.

The former results do not give any indication of the consistency of the filters. For this, the average NIS test was used. The comparison is presented in Fig. 2. All filters were found to become consistent within less than 5 seconds, with the initial inconsistency caused by the error introduced in the attitude initialization.

B. Experiment

The proposed approach was further validated through an experiment. An IMU and two UWB receivers were mounted on a rigid body, shown in Fig. 3, with the two UWB receivers placed 1.80 m apart. Five UWB anchors were placed at various heights around a room where the experiments were conducted. Trials of approximately two minutes were
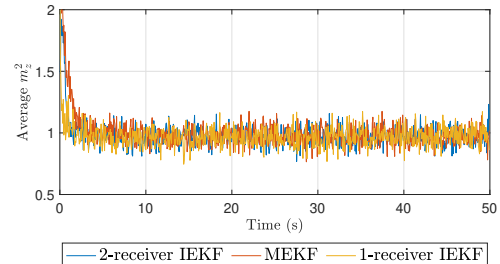

Fig. 2. Comparison of simulation normalized average NIS for two-receiver IEKF, MEKF and one-receiver IEKF for 100 Monte Carlo runs.
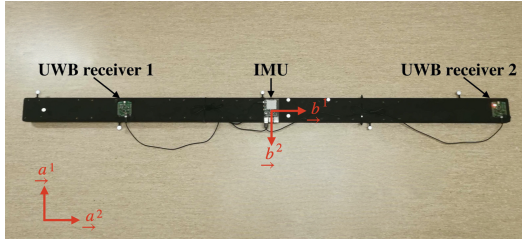
Fig. 3. Experimental setup. Two UWB position receivers and one IMU mounted on a rigid body that is moved by hand to collect data.

recorded, during which the rigid body was moved around a volume measuring 5 m × 4 m × 2 m. A motion capture system was used to record ground truth measurements. The accelerometer and gyroscope measurements were collected at a frequency of 250 Hz, while the UWB position measurements arrived at a frequency of about 17 Hz.

The process noise power spectral density (PSD) matrices were computed using the Allan variance method, generated using static IMU data, according to [24]. The measurement noise covariance matrix was computed through comparison of the recorded measurements and motion capture ground truth measurements. The resulting PSD and covariance matrices are

$$\boldsymbol{Q}(t) = \text{diag}\Big(\boldsymbol{Q}^\omega(t), \boldsymbol{Q}^{\text{a}}(t)\Big), \tag{38}$$

$$\boldsymbol{Q}^\omega(t) = \text{diag}\Big(2.0^2, 2.0^2, 1.8^2\Big) \times 10^{-4} \; (\text{rad})^2, \tag{39}$$

$$\boldsymbol{Q}^{\text{a}}(t) = \text{diag}\Big(1.7^2, 1.5^2, 2.4^2\Big) \times 10^{-2} \; (\text{m/s}^2)^2, \tag{40}$$

$$\mathbf{R} = \text{diag}\Big(\mathbf{R}^{z_1 w}, \mathbf{R}^{z_2 w}\Big), \tag{41}$$

$$\mathbf{R}^{z_1 w} = \text{diag}\Big(1.3^2, 1.1^2, 1.9^2\Big) \times 10^{-2} \; (\text{m})^2, \tag{42}$$

$$\mathbf{R}^{z_2 w} = \text{diag}\Big(1.9^2, 1.6^2, 2.6^2\Big) \times 10^{-2} \; (\text{m})^2. \tag{43}$$

As in simulation, the attitude was initialized with an error of $\pi/3$ (rad) to demonstrate the advantage of the IEKF in situations in which there is large uncertainty on the initial attitude. The RMSE for each of the filters is presented in Fig. 4. It should be noted that ground truth velocity was not measured directly, but rather computed using the ground truth positions. This process introduces some error into the ground truth velocity, which is used to compute the error in the velocity estimates.

The filter performance on experiment data emulates the simulation performance. The two-receiver IEKF attitude estimate improves greatly over the single-receiver IEKF, but show only slight improvement over the two-receiver MEKF. This improvement arises in the transient phase where the effect of having state-dependent Jacobians impacts the MEKF but not the IEKF. The two-receiver IEKF and MEKF perform equivalently at steady state, which is consistent with previous literature. It should be noted that a transient phase does not only occur during initialization, but can also occur if a sensor is unavailable (that is, "drops out") for an extended period of time.
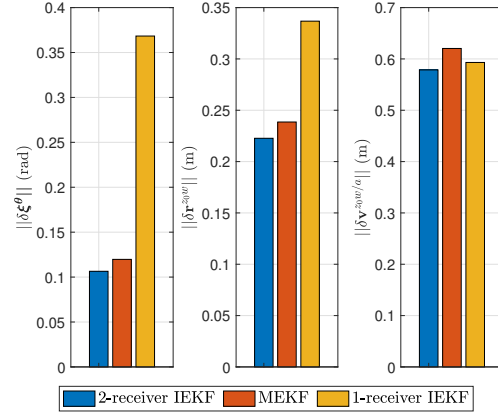

Fig. 4. Comparison of experiment RMSE in attitude, position, and velocity for two-receiver IEKF, MEKF, and one-receiver IEKF.
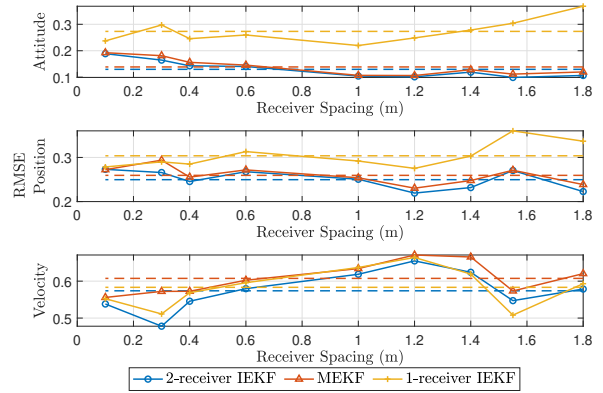

Fig. 5. RMSE of each filter and the two-receiver IEKF in attitude, position, and velocity for various tag spacings.

C. Receiver Spacing Study

The distance between receivers was studied experimentally using the platform shown in Fig. 3. The receiver placement was decreased between experimental runs. For each of the experiment runs, the three filters were compared using RMSE as a performance metric. The resulting RMSEs of each filter are shown in Fig. 5. While reporting the single-receiver IEKF performance as a function of receiver spacing may seem imprecise, the receiver spacing is used to categorize the various experiment runs. While the RMSE of the single-receiver should be consistent across runs, certain inconsistencies arise from factors such as the manual trajectory generation and hardware flaws during data collection. Thus, the single-receiver RMSE are computed and reported for each run. The same data is presented in terms of percent differences between each filter and the two-receiver IEKF in Fig. 6.

The two-receiver IEKF has the greatest advantage over the single-receiver IEKF in attitude estimates, in which a maximum improvement of 110%, and a minimum improvement of 23% was observed. With greater receiver spacing, the advantage introduced by the addition of a second receiver becomes increasingly evident in the position and attitude estimates. Even with the receivers spaced 0.1 m apart, the addition of a second receiver enhances the attitude estimates by 23%, and
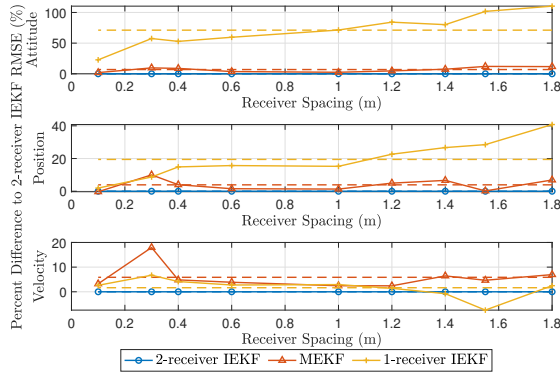
Fig. 6. Percent difference between RMSE of each filter and the two-receiver IEKF in attitude, position, and velocity for various tag spacings.
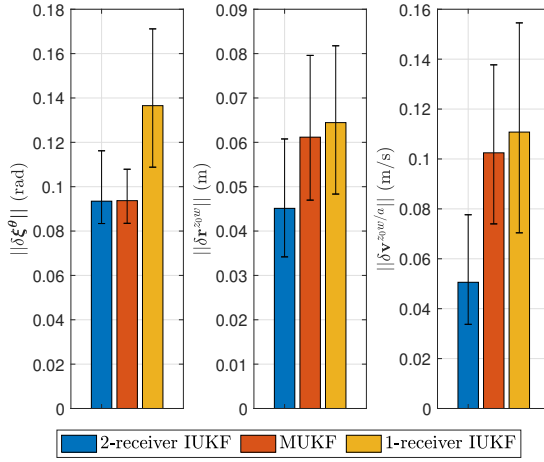

Fig. 7. Attitude, position, and velocity RMSE for two-receiver IUKF and MUKF, as well as one-receiver IUKF, for 100 simulated Monte Carlo runs.

the position estimates by 2%. Over all spacings, the two-receiver IEKF performance improved attitude estimates by 71% over the single-receiver IEKF and by 7% over the two-receiver MEKF. The position estimates were improved by 19% over the single-receiver IEKF and 4% over the two-receiver MEKF.

D. Extension to the Unscented Kalman Filtering Framework

While the focus of this work is on the use of the IEKF, the invariant measurement, invariant error, invariant innovation, and group-affine process model can be used within an invariant UKF (IUKF) framework [25]. Simulation results comparing the performance of the two-receiver IUKF, the two-receiver multiplicative UKF (MUKF), and the single-receiver IUKF are presented in Fig. 7, without a derivation of the filter equations. The derivation of the filters equations follows that of [25].

The average RMSE in attitude of the IUKF is slightly lower than that of the UKF, but the IUKF has slightly larger upper and lower percentile bounds than the UKF. The IUKF definitively outperforms the MUKF in terms of position and velocity RMSE. Also, given the same parameters, the three UKF variants, with results presented in Fig. 7, outperform the corresponding EKF variant, with results presented in Fig. 1.

Therefore, should adequate computing resources be available such that a UKF variant can be used, and performance beyond what the two-receiver versions of the MEKF, MUKF, and IEKF can provide is required, the IUKF is attractive.

V. CONCLUSION

This paper's novel contribution is demonstrating how to use the IEKF to estimate position, velocity, and attitude, that being the extended pose, using two position receivers and IMU data. The two-receiver problem is shown to be left invariant, and all other requirements of the invariant framework are met, enabling the use of the IEKF. The proposed two-receiver IEKF is compared in simulation and experiment to a two-receiver MEKF and a single-receiver IEKF. The two-receiver IEKF was found to have improved performance over the MEKF when the initialization error was large, as is consistent with literature.

APPENDIX

A. MEKF

The kinematics in (17), (18), (19) are framed in the multiplicative extended Kalman filter (MEKF) framework. Here, the linearized process model is of the form,

$$\delta \dot{\mathbf{x}} = \mathbf{A}_c \delta \mathbf{x} + \mathbf{L}_c \delta \mathbf{w}, \tag{44}$$

where

$$\delta \mathbf{x} = \left[\begin{array}{ccc} \delta \boldsymbol{\xi}^{\theta^\mathsf{T}} & \delta \mathbf{v}_a^{z_0 w/a^\mathsf{T}} & \delta \mathbf{r}_a^{z_0 w^\mathsf{T}} \end{array} \right]^\mathsf{T}, \tag{45}$$

and $\exp(\delta \boldsymbol{\xi}^{\theta^\times}) = \mathbf{C}_{ab} \hat{\mathbf{C}}_{ab}^\mathsf{T}$, $\delta \mathbf{v}_a^{z_0 w/a} = \mathbf{v}_a^{z_0 w/a} - \hat{\mathbf{v}}_a^{z_0 w/a}$, and $\delta \mathbf{r}_a^{z_0 w} = \mathbf{r}_a^{z_0 w} - \hat{\mathbf{r}}_a^{z_0 w}$. The process model Jacobians are then

$$\mathbf{A}_c = \left[\begin{array}{ccc} -\mathbf{u}_b^{1^\times} & \mathbf{0} & \mathbf{0} \\ -\hat{\mathbf{C}}_{ab} \mathbf{u}_b^{2^\times} & \mathbf{0} & \mathbf{0} \\ \mathbf{0} & \mathbf{1} & \mathbf{0} \end{array} \right], \quad \mathbf{L}_c = \left[\begin{array}{ccc} -\mathbf{1} & \mathbf{0} & \mathbf{0} \\ \mathbf{0} & -\hat{\mathbf{C}}_{ab} & \mathbf{0} \\ \mathbf{0} & \mathbf{0} & \mathbf{0} \end{array} \right]. \tag{46}$$

Note that both $\mathbf{A}_c$ and $\mathbf{L}_c$ are state dependent.

The MEKF measurement models are identical to those used in the IEKF, with

$$\left[\begin{array}{c} \mathbf{y}_k^1 \\ \mathbf{y}_k^2 \end{array} \right] = \left[\begin{array}{c} \mathbf{y}_k^{\mathrm{pos},1} \\ \mathbf{y}_k^{\mathrm{rel}} \end{array} \right] = \left[\begin{array}{c} \mathbf{r}_{a_k}^{z_1 w} + \mathbf{n}_k^1 \\ \mathbf{r}_{a_k}^{z_2 w} - \mathbf{r}_{a_k}^{z_1 w} + \mathbf{n}_k^1 + \mathbf{n}_k^2 \end{array} \right]. \tag{47}$$

The MEKF innovation is then

$$\delta \mathbf{y} = \left[\begin{array}{c} \mathbf{r}_{a_k}^{z_1 w} + \mathbf{n}_k^1 - \check{\mathbf{C}}_{ab} \mathbf{r}_b^{z_1 z_0} - \check{\mathbf{r}}_a^{z_0 w} \\ \mathbf{r}_{a_k}^{z_2 w} - \mathbf{r}_{a_k}^{z_1 w} + \mathbf{n}_k^1 + \mathbf{n}_k^2 - \check{\mathbf{C}}_{ab} \mathbf{r}_b^{z_2 z_1} \end{array} \right], \tag{48}$$

which can be linearzied and written in the form

$$\delta \mathbf{y}_k = \mathbf{H}_k \delta \mathbf{x}_k + \mathbf{M}_k \delta \mathbf{n}_k, \tag{49}$$

where

$$\mathbf{H}_k = \left[\begin{array}{ccc} \check{\mathbf{C}}_{ab_k} \mathbf{r}_b^{z_1 z_0 \times} & \mathbf{0} & \mathbf{1} \\ \check{\mathbf{C}}_{ab_k} \mathbf{r}_b^{z_2 z_1 \times} & \mathbf{0} & \mathbf{0} \end{array} \right], \quad \mathbf{M}_k = \left[\begin{array}{cc} \mathbf{1} & \mathbf{0} \\ \mathbf{0} & \mathbf{1} \end{array} \right]. \tag{50}$$

REFERENCES

[1] A. Barrau and S. Bonnabel, "A mathematical framework for IMU error propagation with applications to preintegration," in *IEEE International Conference on Robotics and Automation*, 2020, pp. 5732–5738.

[2] C. E. Cohen, "Attitude determination," in *Global Positioning System: Theory and App.* B. W. Parkinson and J. J. J. Spilker, Eds., vol. 2, Reston, VA: AIAA, 1996, pp. 519–538.

[3] R. Hirokawa and T. Ebinuma, "A low-cost tightly coupled GPS/INS for small UAVs augmented with multiple GPS antennas," *Navigation*, vol. 56, no. 1, pp. 35–44, Mar. 2009.

[4] P. Buist, P. Teunissen, G. Giorgi, and S. Verhagen, "Multiplatform instantaneous GNSS ambiguity resolution for triple- and quadruple-antenna configurations with constraints," *International Journal of Navigation and Observation*, vol. 2009, Jan. 2009.

[5] G. Emel'yantsev, B. Blazhnov, and A. Stepanov, "Specific features of constructing a dual-mode GNSS gyrocompass as a tightly-coupled integrated system," *Gyroscopy and Navigation*, vol. 9, pp. 97–105, 2018.

[6] E.-H. Shin, "Estimation techniques for low-cost inertial navigation," PhD thesis, University of Calgary, 2005.

[7] J.-H. Yoon and H. Peng, "A cost-effective sideslip estimation method using velocity measurements from two GPS receivers," *IEEE Transactions on Vehicular Technology*, vol. 63, no. 6, pp. 2589 –2599, Dec. 2013.

[8] Y. Hao, A. Xu, X. Sui, and Y. Wang, "A modified extended Kalman filter for a two-antenna GPS/INS vehicular navigation system," *Sensors*, vol. 18, p. 3809, Nov. 2018.

[9] A. Barrau and S. Bonnabel, "The invariant extended Kalman filter as a stable observer," *IEEE Transactions on Automatic Control*, vol. 62, no. 4, 2017.

[10] S. Särkkä, *Bayesian Filtering and Smoothing*. Cambridge University Press, 2013.

[11] A. Barrau and S. Bonnabel, "Three examples of the stability properties of the invariant extended Kalman filter," *IFAC-PapersOnLine*, vol. 50, no. 1, pp. 431–437, Jul. 2017.

[12] J. Arsenault, "Practical considerations and extensions of the invariant extended Kalman filtering framework," Master's thesis, McGill University, 2019.

[13] P. Richardson, W. Xiang, and D. Shan, "An outdoor UWB tracking system to improve safety of semi-autonomous vehicle operations," *International Journal of Ultra Wideband Communications and Systems*, vol. 1, Feb. 2010.

[14] T. Nageli, B. Hepp, and O. Hilliges, "Omni-directional person tracking on a flying robot using occlusion-robust ultra-wideband signals," in *International Conference on Intelligent Robots and Systems*, Oct. 2016, pp. 189–194.

[15] B. C. Hall, *Lie Groups, Lie Algebras, and Representations*, 2nd ed. Springer, 2014.

[16] C Van Loan, "Computing integrals involving the matrix exponential," *IEEE Transactions on Automatic Control*, vol. 23, no. 3, pp. 424–440, 1978.

[17] Y. Bar-Shalom, X. R. Li, and K. Thiagalingam, *Estimation with Applications to Tracking and Navigation*. Wiley, 2001.

[18] Z. Chen, C. Heckman, S. Julier, and A. Nisar, "Weak in the NEES?: Auto-tuning Kalman filters with Bayesian optimization," in *Fusion*, Jul. 2018.

[19] A. Barrau and S. Bonnabel, "An EKF-SLAM algorithm with consistency properties," 2015. arXiv: `1510.06263`.

[20] A. Barrau, "Non-linear state error based extended Kalman filters with applications to navigation," PhD thesis, Mines Paristech, Paris, France, 2015.

[21] S. Heo and C. G. Park, "Consistent EKF-based visual-inertial odometry on matrix Lie group," *IEEE Sensors Journal*, vol. 18, no. 9, pp. 3780–3788, 2018.

[22] R. Schmalzried, *The Role of RTK in the Autonomous System Sensor Suite*. Swift Navigation, 2017.

[23] J. A. Farrell, *Aided Navigation*. McGraw-Hill, 2008.

[24] O. J. Woodman, *An Introduction to Inertial Navigation*. University of Cambridge, Tech. Report 696, 2007.

[25] M. Brossard, S. Bonnabel, and J.-P. Condomines, "Unscented Kalman filtering on Lie groups," in *International Conference on Intelligent Robots and Systems*, Sep. 2017, pp. 2485–2491.